Theory of enhanced Raman scattering for circular stratified semiconductor cylinder

2007 J. Phys.: Condens. Matter 19 246222

(http://iopscience.iop.org/0953-8984/19/24/246222)

IOP PUBLISHING JOURNAL OF PHYSICS: CONDENSED MATTER

J. Phys.: Condens. Matter **19** (2007) 246222 (8pp) doi:10.1088/0953-8984/19/24/246222

Theory of enhanced Raman scattering for circular stratified semiconductor cylinder

Hui Wang[1], **Min Feng**[1], **Xuewei Cao**[1], **Yufang Wang**[1,2,3] **and Guoxiang Lan**[1,2]

[1] Department of Physics, Nankai University, Tianjin 300071, People's Republic of China
[2] N&T Joint Academy, Tianjin 300071, People's Republic of China

E-mail: yfwang@nankai.edu.cn

Received 16 July 2006, in final form 10 April 2007
Published 25 May 2007
Online at stacks.iop.org/JPhysCM/19/246222

Abstract

Based on the electrodynamic theory, we have calculated the scattering fields of infinitely long dielectric nanocylinders with silver coating, and compared them with those of a pure silicon cylinder. The calculation result indicates that there exists an enhanced electric field in the silver-coated silicon nanocylinder and shows a great Raman enhancement factor ($\sim 10^{12}$) as compared with bulk silicon. For a special area in the silver-coated silicon nanocylinder, the enhancement comes up to 4×10^{13}.

(Some figures in this article are in colour only in the electronic version)

1. Introduction

Since its discovery, surface-enhanced Raman scattering (SERS) has attracted enormous attention of both experimentalists and theoreticians [1–3]. This phenomenon, SERS, can be observed for a variety of molecules when they are adsorbed onto some special prepared substrates. Silver colloids exhibit a very large enhancement factor, 14–15 orders of magnitude, and observations of single molecule Raman scattering are achieved [4–6]. Physical and chemical contributions to surface enhanced Raman scattering were analysed [7–10].

Recently, Cao *et al* [11] have reported a strong Raman scattering enhancement factor, three orders of magnitude, from individual silicon nanowires and nanocones as compared with bulk Si. Although silicon is an indirect bandgap semiconductor and so has low luminescence efficiency, silicon nanocrystals can enhance luminescence efficiency greatly [12]. It is meaningful for semiconductor electronics and silicon-based technology to obtain a great electric field enhancement from semiconductors, particularly from silicon.

The aim of this paper is to propose a scenario that combines both surface enhanced Raman scattering and the effects of structural resonances on Raman scattering. Within the

[3] Author to whom any correspondence should be addressed.

framework of electrodynamics we investigate the propagation of electromagnetic waves in silicon nanocylinders in order to see if the capacity of silver films to enhance optical fields is retained when the surface of a silicon cylinder is coated with it. As an example we consider an infinitely long circular cylinder illuminated by a transverse magnetic (TM) plane wave, and the polarization vector of the incident wave is parallel to the axis of the circular cylinder. The Raman enhancement factors were examined for silver coated and uncoated silicon nanocylinders with different laser-excitation wavelengths. For appropriate conditions, the enhancement approaches 10^{12} as compared with bulk single-crystalline Si (c-Si). It is found that the Raman enhancement depends sensitively on the radius of the silicon cylinder, the thickness of the silver coating, and the excitation wavelengths.

2. Theoretical analysis

The problem of scattering of plane electromagnetic waves by an isotropic circular cylinder has been discussed in detail by Van de Hulst [13]. In figure 1, the coordinates, the electric and magnetic field vectors ($\boldsymbol{E}$ and $\boldsymbol{H}$), and incident wavevector $\boldsymbol{k}_0$ are depicted. Here we give a simple discussion for scattering of a TM plane wave. For a TM plane wave, the following equations (1)–(3) represent the solution of the scalar wave equation for different regions of figure 1 [13, 14].

$$(r > b) \qquad u = \sum_{n=-\infty}^{\infty} \left[J_n(m_0 k_0 r) - b_n^0 H_n(m_0 k_0 r) \right] \tag{1}$$

$$(b > r > a) \qquad u = \sum_{n=-\infty}^{\infty} \left[B_n^1 J_n(m_1 k_0 r) - b_n^1 H_n(m_1 k_0 r) \right] \tag{2}$$

$$(r < a) \qquad u = \sum_{n=-\infty}^{\infty} B_n^2 J_n(m_2 k_0 r), \tag{3}$$

where $J_n(m_i k_0 r)$ and $H_n(m_i k_0 r)$ denote the Bessel function of the first kind and the Hankel function, respectively. Due to boundary conditions, mu and $m\partial u/\partial r$ must be continuous at the interface $r = a$ and the surface $r = b$, respectively, and these result in the following set of equations:

$$b_n^0 m_0 H_n(m_0 k_0 b) - b_n^1 m_1 H_n(m_1 k_0 b) + B_n^1 m_1 J_n(m_1 k_0 b) + 0 = m_0 J_n(m_0 k_0 b) \tag{4a}$$

$$b_n^0 m_0^2 H_n'(m_0 k_0 b) - b_n^1 m_1^2 H_n'(m_1 k_0 b) + B_n^1 m_1^2 J_n'(m_1 k_0 b) + 0 = m_0^2 J_n'(m_0 k_0 b) \tag{4b}$$

$$0 - b_n^1 m_1 H_n(m_1 k_0 a) + B_n^1 m_1 J_n(m_1 k_0 a) - B_n^2 m_2 J_n(m_2 k_0 a) = 0 \tag{4c}$$

$$0 - b_n^1 m_1^2 H_n'(m_1 k_0 a) + B_n^1 m_1^2 J_n'(m_1 k_0 a) - B_n^2 m_2^2 J_n'(m_2 k_0 a) = 0, \tag{4d}$$

where the prime superscript ($'$) denotes the differential of a function with respect to the argument. So coefficient B_n^2 is given as follows:

$$B_n^2 = \frac{\begin{vmatrix} m_0 H_n(m_0 k_0 b) & -m_1 H_n(m_1 k_0 b) & m_1 J_n(m_1 k_0 b) & m_0 J_n(m_0 k_0 b) \\ m_0^2 H_n'(m_0 k_0 b) & -m_1^2 H_n'(m_1 k_0 b) & m_1^2 J_n'(m_1 k_0 b) & m_0^2 J_n'(m_0 k_0 b) \\ 0 & -m_1 H_n(m_1 k_0 a) & m_1 J_n(m_1 k_0 a) & 0 \\ 0 & -m_1^2 H_n'(m_1 k_0 a) & m_1^2 J_n'(m_1 k_0 a) & 0 \end{vmatrix}}{\begin{vmatrix} m_0 H_n(m_0 k_0 b) & -m_1 H_n(m_1 k_0 b) & m_1 J_n(m_1 k_0 b) & 0 \\ m_0^2 H_n'(m_0 k_0 b) & -m_1^2 H_n'(m_1 k_0 b) & m_1^2 J_n'(m_1 k_0 b) & 0 \\ 0 & -m_1 H_n(m_1 k_0 a) & m_1 J_n(m_1 k_0 a) & -m_2 J_n(m_2 k_0 a) \\ 0 & -m_1^2 H_n'(m_1 k_0 a) & m_1^2 J_n'(m_1 k_0 a) & -m_2^2 J_n'(m_2 k_0 a) \end{vmatrix}}. \tag{5}$$

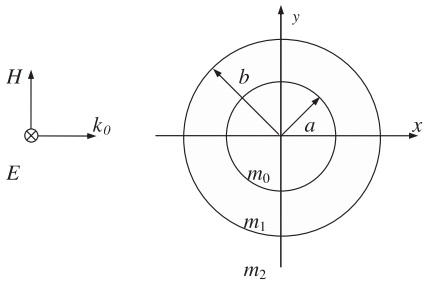

Figure 1. Coordinates and vectors for scattering by concentric infinitely long cylinders; a and b are radii of the inner and outer cylinders; m_0, m_1 and m_2 are the refractive indices in the indicated regions and $\boldsymbol{E}$ and $\boldsymbol{H}$ are the electric and the magnetic vectors of the incident plane wave, respectively. Here $\boldsymbol{k}_0$ is the wavevector of the incident plane wave.

Therefore the electric field for the $r < a$ region, $E^{\mathrm{TM}}_{\mathrm{inner}}$, is given by

$$E^{\mathrm{TM}}_{\mathrm{inner}} = E_0 \sum_{n=-\infty}^{\infty} (-\mathrm{i})^n B_n^2 J_n(m_2 k_0 r) \mathrm{e}^{\mathrm{i}n\theta} \hat{z}, \tag{6}$$

where E_0 is the amplitude of the incident electric field. By integrating $|E^{\mathrm{TM}}_{\mathrm{inner}}|^2$ over the range $r = 0$ to a, one obtains the volume-averaged intensities of the internal field,

$$\bar{I}^{\mathrm{TM}}_{\mathrm{inner}} = \frac{1}{\pi a^2} \int_0^a \int_0^{2\pi} \left| E^{\mathrm{TM}}_{\mathrm{inner}} \right|^2 r \, \mathrm{d}\theta \, \mathrm{d}r. \tag{7}$$

These integrations can be given by [15]

$$\bar{I}^{\mathrm{TM}}_{\mathrm{inner}} = E_0^2 \sum_{n=-\infty}^{\infty} \left| B_n^2 \right|^2 \left[J_n^2(m_2 k_0 a) - J_{n-1}(m_2 k_0 a) J_{n+1}(m_2 k_0 a) \right]. \tag{8}$$

Let I_0 denote the maximum intensity within bulk single crystal silicon embedded in vacuum provided the incident wave is perpendicular to the surface of the bulk Si. The ratio of $\bar{I}^{\mathrm{TM}}_{\mathrm{inner}}/I_0$ is of great importance here. An enhanced electric field gives rise to an enhanced polarization, and therefore to an enhanced inelastic scattering. The enhancement factor can be approximated as $G = (\bar{I}^{\mathrm{TM}}_{\mathrm{inner}}/I_0)^2$ [16] since the difference between the incident-light frequency ω_0 and Stokes scattering frequency ω is small.

3. Results and discussion for single cylinder

Just let $m_0 = m_1 = 1$, and let k_0 denote the wavenumber in vacuum; equations (1)–(8) represent the case of a single cylinder. Thus we can get the absolute intensity for region $r < a$ through equation (8). In figure 2 the enhancement factors for a single silicon cylinder are shown, as functions of radius for 785, 632.8 and 514.5 nm laser excitation wavelengths, respectively. It is clear that the volume-averaged intensities depend on the radius of the cylinder.

It is easy to see that the enhancements exhibit undulations with the radius of the cylinder. For the oscillating period of the Bessel function gradually shortening with increasing argument and eventually taking the value 2π, the enhancement also oscillates with a period approaching $2\pi/4m_2k_0$ [17]. The oscillating periods of enhancement approach 53 nm, 41 nm and 30 nm, respectively, for 785, 632.8 and 514.5 nm excitations. When the radius of the cylinder is near the origin, J_n in equation (8) does not have regular period for different subscripts n, so the enhancement factor gives rise to fine structure. Comparing the three curves in figure 2, the

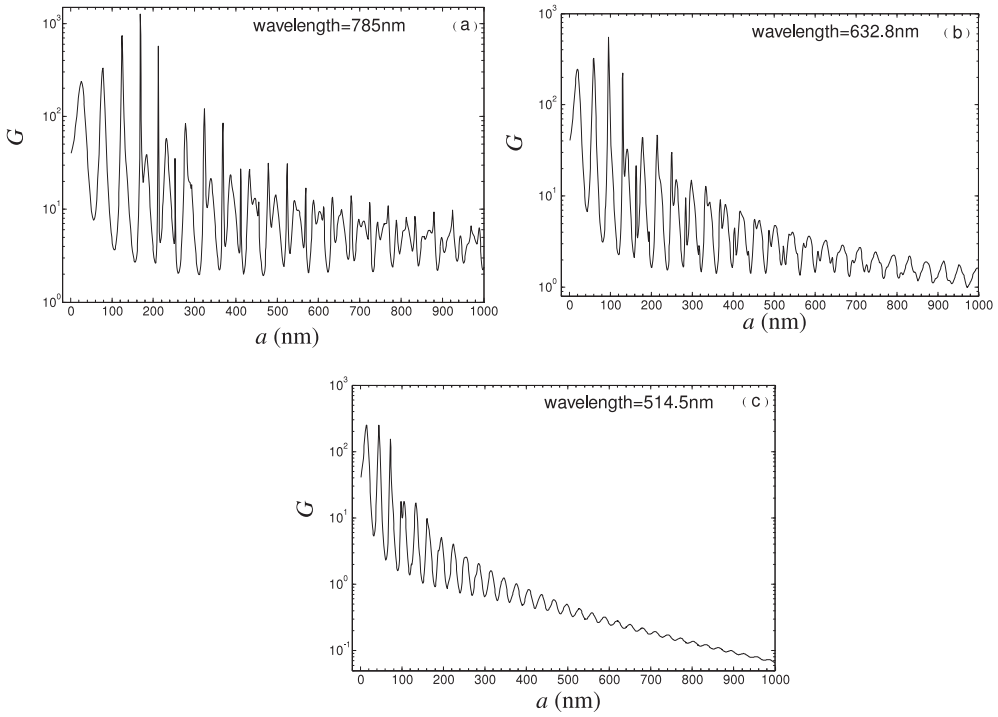

Figure 2. The simulated Raman enhancements based on infinitely long dielectric Si for (a) 785 nm, (b) 632.8 nm, and (c) 514.5 nm wavelength, TM-polarized laser excitation. a, radius of the silicon cylinder; G, enhancement factor.

fine structure occurring in figure 2(c) is the least. The reason is that the imaginary part of the refractive index of silicon for 514 nm wavelength is the largest among the three wavelengths, and it is about three times that for 632.8 nm and eight times for 785 nm.

4. Results and discussion for stratified cylinder

4.1. Calculated results of enhancements

According to equation (8), the enhancement factors for the case of a coated silicon cylinder can be calculated. In figure 3, we show a detailed picture of the enhancements as functions of radius a and silver film thickness t. Clearly when the stratified infinitely long cylinder is embedded in vacuum, the largest enhancement is approximately 4.4×10^{12} for 785 nm wavelength ($a = 145.8$ nm, $t = 17$ nm), 1×10^{12} for 632.8 nm wavelength ($a = 76.6$ nm, $t = 27.1$ nm), 4.3×10^{11} for 514 nm wavelength ($a = 53.4$ nm and $t = 20.9$ nm), respectively.

It can be seen from figure 3 that both silicon and silver contribute to the enhancements. When the thickness of the Ag film is very thin, the effect of enhancement is weak. With increasing silver film thickness, the enhancement factors of Raman scattering increase sharply at first, reach their peaks, and then decrease gradually.

4.2. Corresponding natural modes

The rectangular components of the vector potential all satisfy the eigenequation [18]

$$\nabla^2\phi + k^2\phi = 0. \tag{9}$$

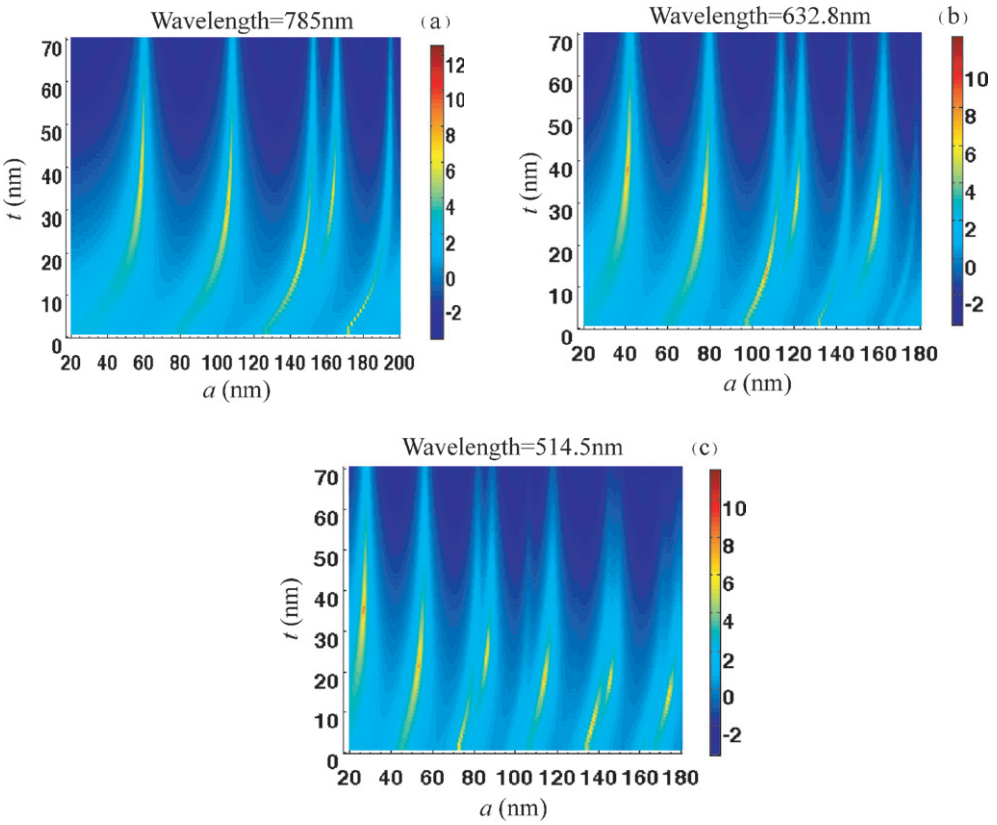

Figure 3. Dependences of the enhancement factors on the radius and thickness for (a) 785 nm, (b) 632.8 nm and (c) 514.5 nm with TM-polarized laser excitation. a, radius of the inner cylinder of silicon; t, thickness of silver film; the colour bar in each picture represents the values of $\log_{10}(G)$.

There exists a nontrivial function ϕ satisfying equation (9) throughout the whole space and vanishing at infinity. Under the configuration shown in figure 1, the function ϕ must be chosen by letting the fields satisfy the radiation condition and the boundary conditions [18]. Thus we obtain a system of four simultaneous equations which are linear and homogeneous in the four expansion coefficients of the fields (for detailed discussion see [18]). The compatibility condition is

$$\Delta \equiv \begin{vmatrix} m_0 H_n(m_0 k_0 b) & -m_1 H_n(m_1 k_0 b) & m_1 J_n(m_1 k_0 b) & 0 \\ m_0^2 H_n'(m_0 k_0 b) & -m_1^2 H_n'(m_1 k_0 b) & m_1^2 J_n'(m_1 k_0 b) & 0 \\ 0 & -m_1 H_n(m_1 k_0 a) & m_1 J_n(m_1 k_0 a) & -m_2 J_n(m_2 k_0 a) \\ 0 & -m_1^2 H_n'(m_1 k_0 a) & m_1^2 J_n'(m_1 k_0 a) & -m_2^2 J_n'(m_2 k_0 a) \end{vmatrix} = 0. \tag{10}$$

The roots of equation (10) are discrete and determine the natural modes of an infinitely long cylinder. The Bessel functions are transcendental; thus for each value of subscript n there is a denumerable infinity of roots, any one of which can be denoted by the subscript i. Every root of equation (10) can then be designated by n_i. For our calculations we have used the refractive indices of bulk silicon and silver as tabulated in [19], and let $m_0 = 1$. Since the radii of the inner and outer cylinders, a and b, are real numbers, equation (10) cannot be satisfied precisely. In the case of 785 nm excitation wavelength, the absolute values of Δ in equation (10) for different subscripts n are shown in figure 4.

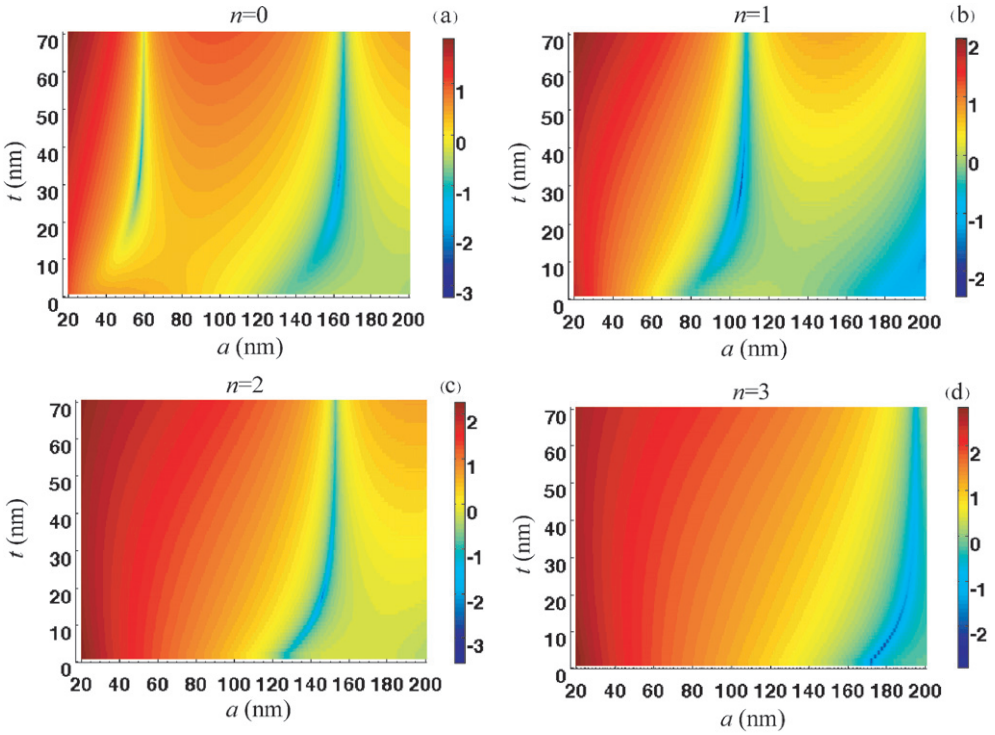

Figure 4. The magnitude of $\log_{10}(\Delta)$ of 785 nm excitation wavelength for (a) $n = 0$, (b) $n = 1$, (c) $n = 2$ and (d) $n = 3$, respectively. a, radius of the inner cylinder; t, thickness of silver film; the colour bar in each picture represents the values of $\log_{10}(G)$.

As shown in figure 4, there exist several channels. Every channel approaches a certain natural mode. In figure 4(a), the left channel approaches the $n_i = 0_0$ natural mode; the right one approaches 0_1 natural mode. The channels in figures 4(b)–(d) approach the 1_0, 2_0 and 3_0 natural modes, respectively. It is easy to see that every channel in figure 4 corresponds to an upheaval in figure 3(a). So the upheavals of enhancement factors in figure 3 originate from corresponding natural modes which enhance the inner electric fields. All the above discussions are also valid for 632.8 and 514.5 nm wavelengths.

For the case of 785 nm wavelength, when $a = 145.8$ nm and $t = 17$ nm, approaching the $n_i = 2_0$ natural mode, the inner electric field distribution of the silicon cylinder is shown in figure 5. Under the above conditions, the enhancement factor reaches its peak, 4.4×10^{12}, and it is called the whispering-gallery mode (WGM) [20–22]. The whispering-gallery mode greatly enhances the inner electric field of the cylinder, and the largest electric field occurs at $r = 107$ nm along the x and y axes; the corresponding enhancement around these points can reach 4×10^{13}.

From the above results, it is found that silver-coated silicon cylinder gives a tremendous enhancement factor ($\sim 10^{12}$), which is roughly eight orders of magnitude higher than that of a single circular cylinder. The combination of silver and silicon results in this great enhancement, which can be attributed to the localized surface plasmon excitations. The resonance peak of metal-coated dielectric nanoparticles shifts dramatically from those of bulk metal. In addition, the reduced mean free path of conduction electrons in the metal shell results in the broadening of the plasmon peak. In fact, large plasmon peak shifts, from ~650 to ~900 nm, were observed

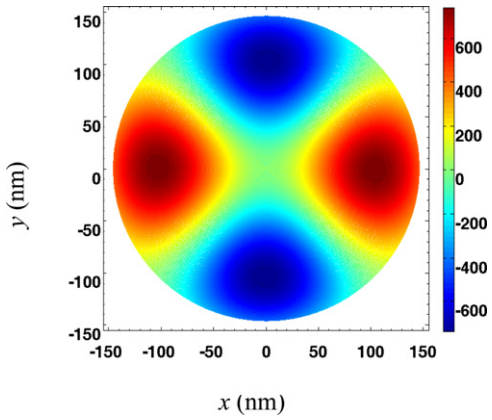

Figure 5. Inner electric field distribution of silver-coated silicon cylinder illumined by 785 nm excitation wavelength when a is 145.8 nm and t is 17 nm; the values of electric fields are depicted by the colour bar. The amplitude of the incident electric field E_0 is assumed to be unity.

in Au-coated Au_2S nanoshells [23], and the surface plasmon peak of Ag–Pd nanostructures can be tuned from 440 to 730 nm and the peak width can be greatly broadened [24]. The peak shift is dependent upon both the dimensions and the dielectric properties of the nanoparticles, and the experimental results are consistent with the theoretical analysis.

5. Summary

Using the scattering field theory, we are able to investigate the enhancement effects of silver coated and uncoated silicon cylinders. The resonance effects can be obtained for both cases, especially for the silver coated cylinder. Under appropriate conditions, the enhancement factor is as high as $\sim 10^{12}$. The large enhancements are attributed to the localized surface plasmon excitations. The theoretical results presented in this paper can be used to expand the application areas of silicon and silicon-based nanomaterials. This can be directly applied to other dielectric media and further generalized for the case of any arbitrary number of concentric cylinders.

Acknowledgments

This project is supported by the CEM Foundation for N&T Joint Academy (Chinese Education Ministry Foundation for Nankai University and Tianjin University Joint Academy) and the Basic and Applied Research Foundation of Tianjin (contract No 07JCYBJC00400).

References

[1] Fleischmann M, Hendra P J and McQuillan A 1974 *Chem. Phys. Lett.* **26** 163
[2] Jeanmarie D L and Duyne R P V 1977 *J. Electroanal. Chem.* **84** 1
[3] Albrecht M G and Creighton J A 1997 *J. Am. Chem. Soc.* **99** 5215
[4] Nie S and Emory S R 1997 *Science* **275** 21
[5] Kneipp K, Wang Y, Kneipp H, Perelman L T, Itzkan I, Dasari R R and Feld M S 1997 *Phys. Rev. Lett.* **78** 1667
[6] Neacsu C C, Dreyer J, Behr N and Raschke M B 2006 *Phys. Rev.* B **73** 193406
[7] Grand J, delaChapelle M L, Bijeon J L, Adam P M, Vial A and Royer P 2005 *Phys. Rev.* B **72** 033407
[8] Laurent G, Félidj N, Aubard J, Lévi G, Krenn J R, Hohenau A, Schider G, Leitner A and Aussenegg F R 2005 *Phys. Rev.* B **71** 045430

[9] Persson B N J, Zhao K and Zhang Z 2006 *Phys. Rev. Lett.* **96** 207401
[10] Pustovit V N and Shahbazyan T V 2006 *Phys. Rev.* B **73** 085408
[11] Cao L, Nabet B and Spanier J E 2006 *Phys. Rev. Lett.* **96** 157402
[12] Pavesi L, Dal Negro L, Mazzoleni C, FranzoÁ G and Priolo F 2000 *Nature* **408** 440
[13] van de Hulst H C 1957 *Light Scattering by Small Particles* (New York: Wiley)
[14] Kerker M and Matijevic E 1961 *J. Opt. Soc. Am.* **51** 506
[15] Ruppin R 1998 *J. Opt. Soc. Am.* A **15** 1891
[16] Chu L C and Wang S Y 1985 *Phys. Rev.* B **31** 693
[17] Watson G N 1952 *A Treatise on the Theory of Bessel Functions* 2nd edn (Cambridge: Cambridge University Press)
[18] Stratton J A 1941 *Electromagnetic Theory* (New York: McGraw-Hill)
[19] Palik E D 1985 *Handbook of Optical Constants of Solids* (Orlando, FL: Academic)
[20] Oraevsky A N 2002 *Quantum Electron.* **32** 377
[21] Matsko A B and Ilchenko V S 2006 *IEEE J. Quantum Electron.* **12** 3
[22] Deng S Z, Cai W and Astratov V N 2004 *Opt. Express* **12** 6468
[23] Averitt R D, Sarkar D and Halas N J 1997 *Phys. Rev. Lett.* **78** 4217
[24] Chen J, Wiley B, McLellan J, Xiong Y, Li Z-Y and Xia Y 2005 *Nano Lett.* **5** 2058